Experimental and numerical study of a confined variable density turbulent jet submitted to a strongly pulsed coflow

Yannick Bury, Marc Saudreau, Jacques Borée, Georges Charnay

Experimental and numerical study of a confined variable density turbulent jet submitted to a strongly pulsed coflow

Y.Bury, M.Saudreau, J.Borée, G.Charnay

Institut de Mécanique des Fluides de Toulouse. UMR CNRS/INPT-UPS 5502, Av. Camille Soula, 31400 Toulouse, France

Abstract — An experimental and numerical work dedicated to the study of a confined variable density jet subjected to a time-varying coflow with high acceleration/deceleration levels is presented in this paper. A global analysis and a hyperbolic model based on momentum equation written for the centerline excess velocity are first developped to obtain physical understanding and to estimate relevant effects governing such a complex unsteady flow. In order to observe the jet as it interacts with the main flow and to quantify those effects, two-component laser Doppler velocimetry and optical concentration measurements based on Mie scattering are used and adapted to unsteady conditions. Light, heavy and air jets are successively studied. During acceleration phases, convective phenomena govern part of the flow and a front formation appears which strength increases as initial jet density is lower. This front propagates at a constant velocity and deeply modifies mixing processes and mass transfer in comparison with steady coflowing jet. Comparisons with RANS numerical simulations using $k-\epsilon$ model are presented. Agreement with measurements of longitudinal velocity field is acceptable.

1. Introduction

Turbulent mixing of a jet exhausting in a different density coflow is met in numerous industrial situations. The present work is directly linked with development of natural gas vehicles (NGV) which have a high potential to reduce urban air pollution. In such spark ignition engine, the injected gaseous fuel in the intake ports ($\frac{\rho_{fuel}}{\rho_{air}} = 0.55$) is submitted to a pulsed air flow where acceleration can reach $3000g$ values (g is the gravity acceleration field). Knowledge of the mixing processes in those particular unsteady conditions is useful to optimize combustion [1]. Previous study concerning light jet in a pulsed crossflow [2][3][4] has shown the complex 3D influence of this unsteadiness on the global behavior of the jet. In the present work and owing to the complexity of measurements in real engines, a model experiment setup, considering a variable density turbulent jet exhausting in a strongly pulsed coflowing duct flow, has been developped to isolate and analyse the main physical mechanisms governing such unsteady flows. The experimental setup and the measurements techniques, quoted below, will first be described.

A physical analysis based on a global integral approach and a hyperbolic model derived from momentum equation written for the centerline excess velocity will show that the flow is mainly governed by the balance between unsteady and convective effects. This shows a front formation during acceleration phase, convected downstream at a finite velocity, depending on the initial jet density. Buoyancy effects due to the flow acceleration field are found to be globally weak.

Two-component laser Doppler velocimetry and laser planar tomography visualizations adapted to unsteady conditions, as well as $k-\epsilon$ simulations confirm this behaviour. Measurements also bring relevant informations concerning strong modification of turbulence production and anisotropy during acceleration and deceleration phases. Mixing processes and mass transfer are deeply modified by the time-varying coflow, in comparison with corresponding steady coflowing jet.

2. Experimental Setup

2.1. Flows Generation and Main Characteristics

The experimental setup is sketched in figure 2. It consists of a $D = 4mm$ diameter cylindrical tube jet confined in a $60 \times 60mm^2$ transparent square duct. The use of a sonic nozzle ensures a time-constant mass flux jet. Nozzle location is optimized in order to obtain a fully developped turbulent pipe flow with a $U_0 = 60m/s$ axial velocity at the jet exit. The total length of the duct generating the coflow is $2.40m$. The channel flow is generated by a vacuum pump and pulsed thanks to a motorized butterfly valve at a $f = 75Hz$ frequency. Pulsation is tuned with the channel acoustics and corresponds to a half-wave mode [5]. Duct entrance is a pressure node. As a result, for about thirty jet diameters downstream the duct inlet, including test section, coflow velocity U_∞ is quasi-uniform and varies from 5 to $30m/s$ with time (see fig.4). The jet therefore develops in a spatially uniform, time varying coflow. Resulting values of acceleration/deceleration $\dot{U}_\infty$ rise up to $\pm 400g$.

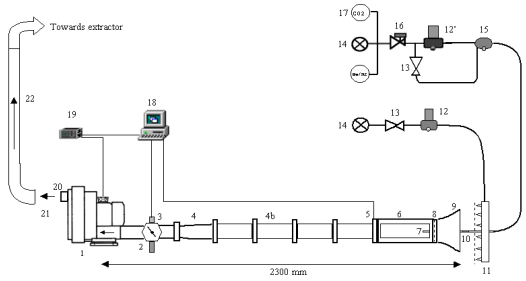

1 Vacuum pump
2 Motorized butterfly
3 Encoder
4 Diffuser
4b Duct module
5 Pressure sensor
6 Test section
7 Coaxial jet
8 Turbulence generating grid
9 Convergent type collector
10 Sonic nozzle
11 « spider » seeding diffusor
12 Seeding system
12' Pressurised seeding system
13 Flow control valve
14 Compressed air
15 Pressure measurement chamber
16 Electropneumatic servocontrol valve
17 CO2 or He/N2 mixing pressurized gas
18 Parameters control computer
19 RFI filter equipped rotation speed switch
20 Exhaust
21 Buffer zone
22 Exhaust circuit

Figure 1: Experimental setup

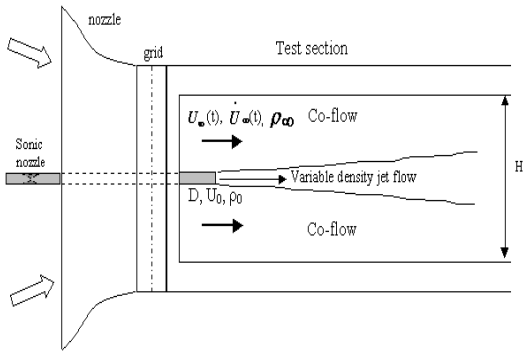

Figure 2: Presentation of the test section

To bring to the fore main effects governing such a flow, light, homogeneous and heavy jets are studied. Density variations are obtained considering an air channel flow and successively air, CO2 ($\frac{\rho_{CO2}}{\rho_{air}} = 1.6$) and an air-helium mixture ($\frac{\rho mix}{\rho_{air}} = 0.55$) jet flow. The corresponding Reynolds numbers, based on outlet jet diameter, vary from $9,000$ to $30,000$, depending on the initial density. The study focuses from 0 to 25 diameters downstream the jet outlet. Particular care has been taken considering experimental boundary conditions, in view of numerical simulation comparison. To do so, a convergent type collector and a grid, placed at the duct entrance (fig.2), just upstream the studying zone, generate uniform coflow velocity profile and isotropic homogeneous turbulence, and minimize the influence of the jet tube's wake.

Duct acoustics was determined by pressure and velocity measurements. In order to observe the jet as it interacts with the main flow and to quantify those effects, two-component laser Doppler velocimetry (Dantec BSA) and optical concentration measurements based on Mie scattering are used and adapted to unsteady conditions. An original pressurized and regulated oil seeding system was specially designed in this way (see fig 1). Considering LDV measurements, coflow and jet flow seeding rates are set equal to limit resulting measurements bias. Considering tomography measurements, only the coaxial jet is seeded. An encoder is connected to the motorized butterfly valve in order to phase average unsteady results. More than 500 samples per encoder degree are used to average LDV data and 200 images for tomography.

Axial velocity measurements from 0 to 25 jet diameters and radial profiles respectively at 0, 5, 10, 15, 20 diameters downstream jet outlet were achieved. For each injected fluid (air, CO2 and air-helium mixture jets), measurements were performed under the four following coflow conditions: Unsteady coflow, steady coflow at respectively $U_\infty = 5m/s$, $U_\infty = 17.5m/s$, $U_\infty = 30m/s$ (corresponding to unsteady phases A, B, C, D in fig.4).

3. Results and Discussion

3.1. Global Analysis

We consider the situation displayed in figure 2. The jet fluid has an ejection velocity U_0 and an initial density ρ_0 possibly very different from the ambient density ρ_∞. The jet flows parallel to the time varying coflow $U_\infty(t)$. The effect of the gravity field g is neglected in all the cases presented in this paper. First, it can easily be checked that the jet Froude number defined by $F_i = \frac{\rho_0 U_0^2}{g|\rho_0 - \rho_\infty| D_0}$ [6] is significantly large. The initial development of the jet is therefore inertial and is not affected by gravity [7][8]. Second, we deal with contrasted situations with $\left|\dot{U}_\infty\right| \gg g$ and $t_p \ll t_g$ where $t_p = \frac{\Delta U_\infty}{\max(\dot{U}_\infty)}$ is the time scale of the pulsation and t_g is the characteristic time scale of the movement induced by gravity along the studying zone length L. The large amplitude variation of the coflow is expected to have a significant effect on the jet behaviour.

A global analysis is based on momentum excess equation integrated over the cross-section of the duct. In an unsteady situation this balance equation writes as follows ([9]) :

$$\underset{(t1)}{\frac{\partial}{\partial t}\iint_{S_j} \rho(U-U_\infty)ds} = \underset{(t2)}{-\frac{\partial}{\partial x}\iint_{S_j} \rho U(U-U_\infty)ds} - \underset{(t3)}{\left[\frac{\partial U_\infty}{\partial t}\right]\iint_{S_j}(\rho-\rho_\infty)ds} \quad (1)$$

In fact a third term, writing $-\frac{\partial U_\infty}{\partial x}\iint_{S_j}\rho(U-U_\infty)ds$, thouroughly appears on the right-hand side of equation (1). This term can be interpreted as the influence of confinement on the flow. However, measurements easily show that this term is negligible for all the cases studied, so we will not take it into account. Equation (1) states that the temporal change of the momentum excess $(t1)$ in a jet slice is due to the longitudinal variation of the excess momentum flux $(t2)$ plus a buoyancy term $(t3)$ if gas density of the jet is different from air density. Phased variations of those terms, for the air-helium jet case at $10D$ and $15D$ downstream the jet outlet, are plotted in figure 3. It may be noted that only terms $(t1)$ and $(t3)$ are directly computed from mean velocity and density fields measurements. The momentum excess flux $(t2)$ is then deduced from balance equation (1) : $(t2) = (t1) - (t3)$.

For distances corresponding to $10D$ and $15D$ downstream the jet outlet, figure 3 shows that during deceleration (from phase 0 to phase 90) the buoyancy term $(t3)$ is negative and contributes to decrease the flow momentum excess. The situation is just the opposite during acceleration (from phase 90 to phase 180). However we can notice that buoyancy effects are weak when compared to convective one. In this way, pulsed flow is globally governed by the balance between convective and temporal variation terms.

During the deceleration phase, the excess momentum flux at the jet exit $J_0(t) = \frac{\pi D^2}{4}.U_0.(U_0 - U_\infty(t))$ considerably increases since the jet flux is time-independant. This excess momentum flux therefore "feeds" excess momentum in the coflowing jet, downstream the jet outlet, and term $(t1)$ is positive. The reverse situation is obtained during acceleration phase. $J_0(t)$ decreases and the longitudinal variation of excess flux "evacuates" excess momentum. Figure 3 shows that

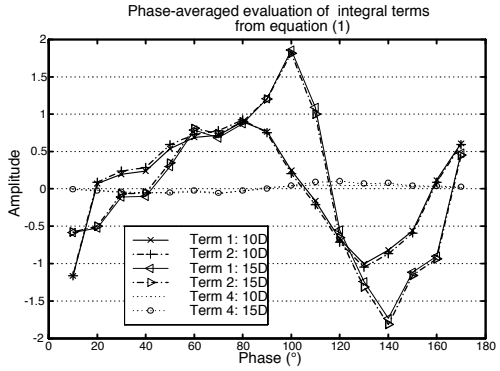

Figure 3: Phased averaged evolution of integral terms from equation (1)

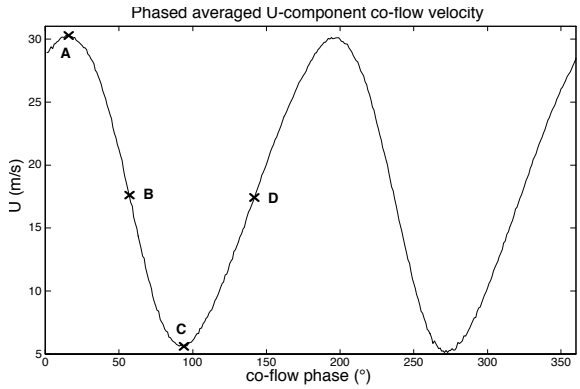

Figure 4: Coflow velocity U_∞ time evolution. (A : $U_\infty(t) = 30$ m/s, B: $U_\infty(t) = 17.5$ m/s deceleration, C: $U_\infty(t) = 5$ m/s and D: $U_\infty(t) = 17.5$ m/s acceleration)

those two sequences do not occur at the same phase for $\frac{x}{D} = 10$ and $\frac{x}{D} = 15$, where x is the downstream distance from the jet outlet. Moreover, comparison with time evolution of coflow velocity $U_\infty(t)$ (fig 4) shows that for $\frac{x}{D} = 15$, a sharp increase of the local excess momentum still occurs at the beginning of the acceleration phase. In fact, considering the axial centerline velocity U_{axis} and quasi-steady situations, one can see that U_{axis} is maximum when the coflow velocity $U_\infty(t)$ is the highest, and minimum when $U_\infty(t)$ is the lowest (see fig.7 and 5). As perturbations are convected at velocity U_{axis}, the excess momentum evacuated downstream focuses during acceleration phase in a starting jet fashion and is responsible for the formation of a velocity front. This behaviour is more formally addressed by studying the local evolution of the excess centerline velocity. A hyperbolic model based on momentum equation for the centerline excess velocity $U_{axis} - U_\infty$ using a simple hypothesis for turbulence closure was obtained. This model will not be detailed here [9] but it shows that the convective nature of the flow is responsible for a focusing on characteristic curves (i.e. the formation of a "shock wave") during acceleration phase only.

The unsteady behavior of the pulsed coflowing jet is seen to be complex but can thus be analysed with fairly general arguments. Time scale comparison can be useful to estimate a priori the unsteadiness "level" of the jet. For a convective phenomenon, $t_{jet} = \frac{x}{U_{axis}}$ is an appropriate time scale for the jet. If $U_{axis} \sim \frac{1}{x}$, t_{jet} sharply increases when one moves downstream. In the present situation, if t_{jet} is evaluated using the steady jet at mid coflow velocity $U_\infty = \frac{30+5}{2} = 17.5m/s$ and compared with $t_p = \frac{1}{2\pi f}$, the time scale of the periodic pulsation ($f = 75Hz$ is the pulsation frequency), $\frac{t_{jet}}{t_p} \sim 1$ for $\frac{x}{D} = 15$. From the jet exit to $10D$ the jet is therefore quasi-static. On the contrary, the region of interest is fully unsteady.

3.2. Local Analysis

The axial evolution of the mean longitudinal velocity at phases A, B, C, D (fig.4) is displayed in figure 5 for the light jet. Each result is then compared with steady coflow velocity measurements in fig.6 and 7. A very large amplitude variation of the axial velocity is detected in figure 5. The axial velocity at phase C, corresponding to the end of the deceleration phase, is much lower than the velocity for a corresponding steady coflow $U_\infty = 5m/s$ (fig.7). On the contrary, the mean axial velocity at the end of the acceleration phase (A) is higher than the velocity for

a corresponding steady coflow $U_\infty = 30m/s$. At phases B and D, the instantaneous coflow velocity seen by the jet is the same (U_∞ =17.5m/s). The acceleration (respectively deceleration) value are however maximum. figure 6 shows that the longitudinal evolutions of axial velocity for phases B and D lie on both sides of the steady coflow case $U_\infty = 17.5m/s$. Similar behaviour is observed for homogeneous and heavy jets.

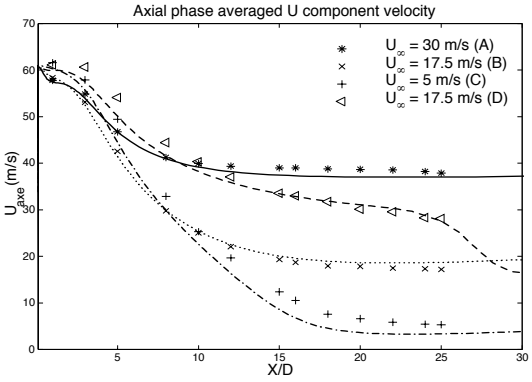

Figure 5: Light jet case comparison of U_{axis} evolution between measurements (symbol) and $k-\epsilon$ simulation (lines)

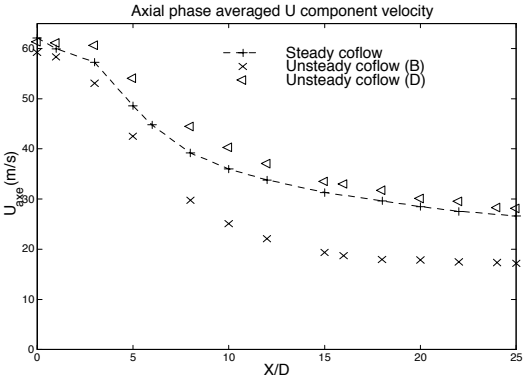

Figure 6: Light jet case comparison of U_{axis} evolution between steady and unsteady coflow for $U_\infty = 17.5$ m/s

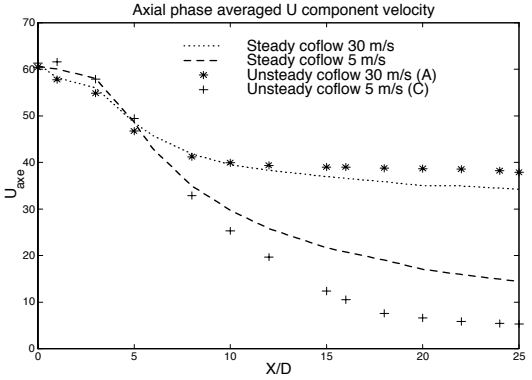

Figure 7: Light jet case comparison of U_{axis} evolution between steady and unsteady coflow for $U_\infty = 5$ m/s and $U_\infty = 30$ m/s

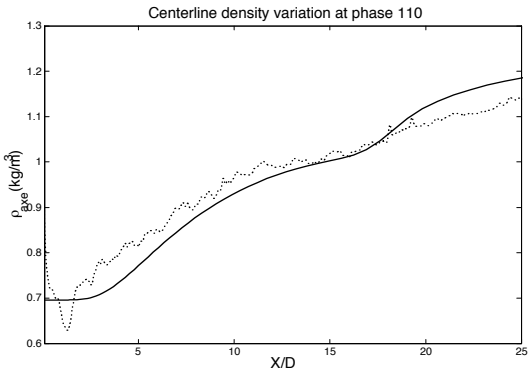

Figure 8: Light jet case comparison of centerline density evolution between measurements (dashed line) and $k-\epsilon$ simulation (solid line)

At a given station downstream jet exit during acceleration or deceleration phase two cumulative effects are present: change in excess momentum flux at the jet outlet and change in the outer pressure gradient needed to accelerate the coflow.

One noticeable feature is the formation of the velocity front during acceleration phase. Signature of front propagation can be obtained by measuring longitudinal velocity U_{axis} (fig 14) and its gradient along jet axis $\frac{\partial U_{axis}}{\partial x}$(fig 9). Measurements show that this front appears during acceleration phase (from phase C to phase D) for $\frac{x}{D} > 15$, which was predicted by dimensional analysis, and propagates at a constant velocity $V_o = 19m/s$ which corresponds to the slope on the (x,t) diagram in figure 9.

As long as we are interested in mixing we may wonder if this behaviour modifies mixing properties of the jet. In figure 10 and 8 are shown phase averaged density fields and centerline

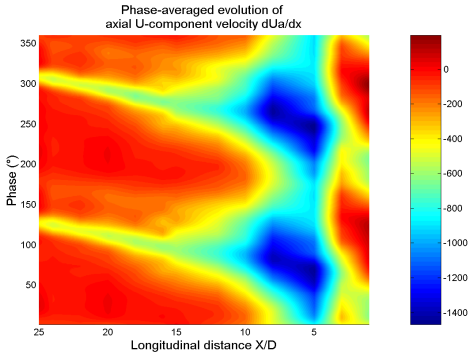

Figure 9: Phased-averaged evolution of long. gradient of U component centerline velocity

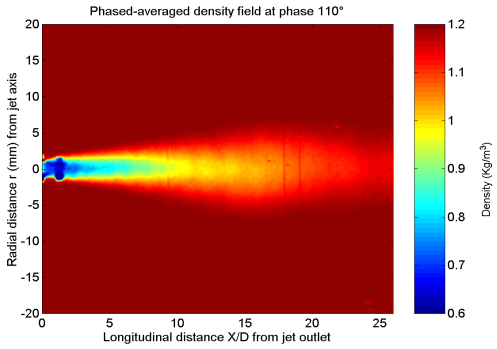

Figure 10: Phase-averaged 2D density field of Air-Helium jet at phase 110^o

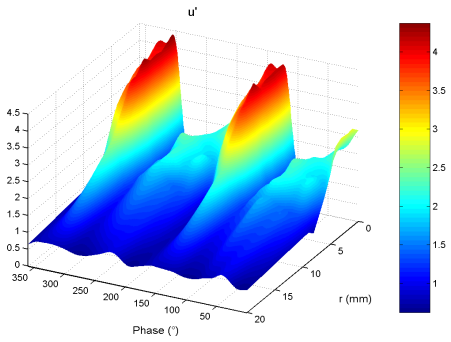

Figure 11: Phased-averaged evolution of radial profile for long. turbulence intensity u'

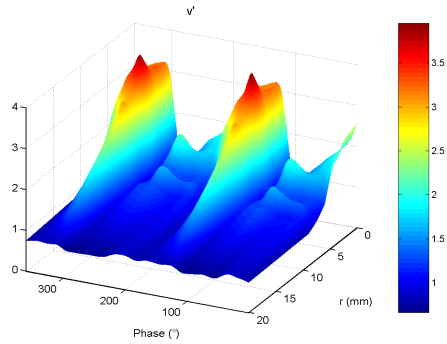

Figure 12: Phased-averaged evolution of radial profile for radial turbulence intensity v'

density profile. As well as centerline velocity U_{axis}, longitudinal density profile presents the same front and indicates an appreciable modification in the jet entrainment and mixing rate. This phenomenon looks like starting jet ([10]) and the head of the perturbation is expected to be a kind of spherical vortex. However in our case, during front formation, ambiant fluid velocity still strongly varies. Thus the front growth is alterated by the outer pressure gradient.

Another important aspect of this front formation is that generated longitudinal gradient velocity $\frac{\partial U_{axis}}{\partial x}$ (fig 9) dramatically increases $< u^2 >$ (fig 11) component via turbulent energy production ([11]). In figure 13 structural parameter introduced by Towsend $k = \frac{u'-v'}{u'+v'}$, where u' (resp. v') is the longitudinal (resp radial) rms velocity, is plotted versus (r, t). Anisotropy is enhanced as the front propagates and decreases behind the front when energy produced on $< u^2 >$component is transferred to $< v^2 >$ and $< w^2 >$components. This strong alternate anisotropy may induce serious problems concerning $k - \epsilon$ modelisation since it is based on isotropic hypothesis. Computations are presently performed with ESTET computer code. Turbulence modelisation, in a Favre averaged formulation, is based on either $k-\epsilon$ or $R_{ij}-\epsilon$ closure schemes [12] and boundary conditions are given by experimental measurements. We present in figures 5,8,15 and 16 first simulation results with standard $k - \epsilon$ model for axisymetric flow ($C_{\epsilon 1} = 1.6$). Figures 15 and 16 show that the phase averaged radial evolution computed with $k-\epsilon$ model are qualitatively correct. More work is presently performed to compare the turbulent field prediction with experiments.

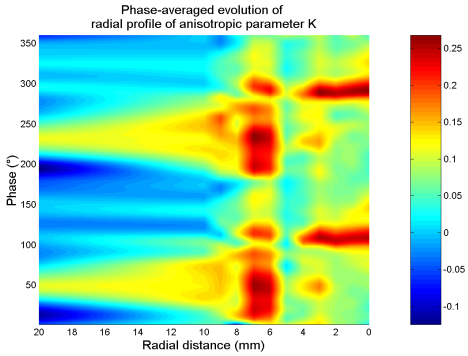

Figure 13: Phased-averaged evolution of radial profile for structural parameter $k = \frac{u'-v'}{u'+v'}$

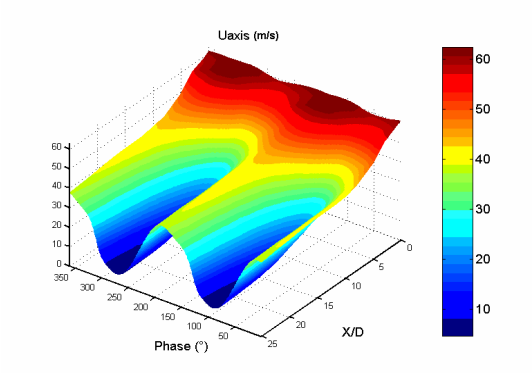

Figure 14: Phased-averaged evolution of long. profile for U component centerline velocity

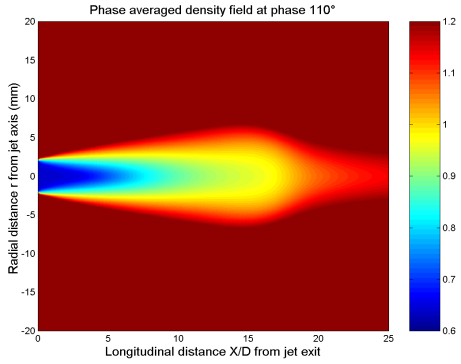

Figure 15: $k-\epsilon$ 2D density field of Air-Helium jet at phase 110^o

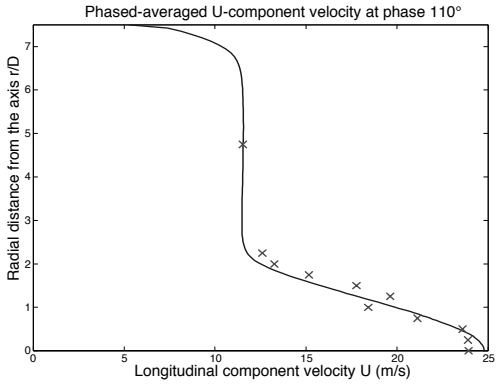

Figure 16: Phased-averaged evolution of radial profile at $\frac{x}{D} = 20$ for longitudinal-component velocity. $k-\epsilon$ simulation (solid line), measurements (dashed line).

3.3. Conclusion

Experimental and numerical investigations based on two-component laser Doppler velocimetry, laser sheet tomography visualizations and $k-\epsilon$ simulations have been performed to study the dynamic behaviour of a variable density jet submitted to a strongly pulsed confined coflow. This configuration modelizes natural gas injection in intake ports of vehicles (NGV). This gaseous fuel has a high potential to reduce urban air pollution. A large part of this work was devoted to isolate and analyse the influence of the unsteady effects on mixing processes and mass transfer between the jet and the coflow.

A first global integral approach and a hyperbolic model based on momentum equation written for centerline excess velocity has been developped to predict the behaviour of the flow. Convective effects globally governe the flow. This shows a front formation during acceleration phase, convected downstream at a finite velocity, depending on the initial jet density. Velocity and density measurements as well as $k-\epsilon$ calculations confirm this. Therefore, mixing is strongly affected by this front. Turbulence production and anisotropy are either deeply modified during acceleration and deceleration phases.

In real engine configurations, as the jet behaviour highly depends on the phase of the pulsed

air flow, the instant of injection will be a crucial parameter for optimization of intake mixing process.

References

1. Fulachier L. Borghi R. Anselmet F. Paranthoen, P. Influence of density variations on the structure of low-speed turbulent flows: a report on euromech 237. *J. Fluid Mech.*, 203:577–593, 1989.
2. Raud N. Bury Y. Bazile R. Borée J. Charnay, G. Behaviour of a variable density heated jet subjected to a pulsated crossflow. *2nd Int. Symp. on Turbulence, Heat and Mass Transfer*, pages 259–268, 1997.
3. Bury Y. Raud N. Bazile R. Borée J. Charnay, G. Jet fortement chauffé soumis à un écoulement instationnaire de conduite. *congrès SFT 97 -Thermique aéronautique et spatiale*, pages 408–413, 1997.
4. Raud N. Bury Y. Bazile R. Borée J. Charnay, G. Experimental study of the behaviour of confined variable density jets in a time varying crossflow. *ASME J. Fluids Eng.*, 121:65–72, 1999.
5. Charnay G. Matthieu, J. Periodic flow in a wind-tunnel produced by rotating shutters. *ASME Journal of Fluids Engineering*, 98:1–6, 1976.
6. Chen C.J. Rodi, W. Vertical turbulent buoyant jets - a review of experimental data. *HMT*, 4 Pergamon, 1980.
7. Chassaing P. Harran G. Joly, L. Density fluctuation correlations in free turbulent binary mixing. *J. Fluid Mech.*, 300:1–40, 1994.
8. Panchapakesan N.R. Lumley, J.L. Turbulence measurements in axisymmetric jet of air and helium. part 2. helium jet. *J. Fluid Mech.*, 246:225–247, 1993.
9. Bury Y. *Etude expérimentale modèle du mélange de carburants gazeux (GNV) dans les moteurs alternatifs du secteur automobile*. PhD thesis, INP Toulouse, 2000.
10. Q. Zhang and H. Johari. Effects on acceleration on turbulent jets. *Phys. Fluids*, 8.
11. Borée J. Atassi N. Charnay G. Taubert, L. Measurements and image analysis of the turbulent field in an axisymmetric jet subject to a sudden velocity decrease. *Experimental Thermal and Fluid Science*, 14.
12. Laurence D. Simonin, O. Numerical implementation of second-moment closures and application to turbulent jets. *Recent Research Advances in the Fluid Mechanics of Turbulent Jets and Plumes, P. A. Davies and M. J. Valente Neves (Editors), Kluwer Academic Publishers*, EDF HE 41/93/047/A:281–294, 1994.